N89-15954

ATTITUDE MOTION OF A NON-ATTITUDE-CONTROLLED CYLINDRICAL SATELLITE *

C. K. WILKINSON †

ABSTRACT

In 1985, two non-attitude-controlled satellites were each placed in a low earth orbit by the Scout Launch Vehicle. The satellites were cylindrical in shape and contained reservoirs of hydrazine fuel. Three-axis magnetometer measurements, telemetered real time, were used to derive the attitude motion of each satellite. Algorithms are generated to deduce possible orientations (and magnitudes) of each vehicle's angular momentum for each telemetry contact. To resolve ambiguities at each contact, a force model was derived to simulate the significant long-term effects of magnetic, gravity gradient, and aerodynamic torques on the angular momentum of the vehicles. The histories of the orientation and magnitude of the angular momentum are illustrated.

* *This work was performed in conjunction with Contract F04701-78-C-0125 for the United States Air Force, Space Division*

† *Principal Engineer, Flight Dynamics Department, Textron Defense Systems*

INTRODUCTION

The Scout Launch Vehicle placed the two satellites into a low earth orbit inclined at 37° to the equator. Approximately one minute after orbit insertion, the Scout-4th-Stage/Satellite-System was despun to about 90 deg/s and the two satellites were separated sequentially. The separation event imparted lateral rates to the vehicles which modified their angular momentums and coning angles. The coning angles just after the separation event were predicted to be approximately 10° and 50° for the respective satellites. Each satellite contained a reservoir of hydrazine fuel amounting to 15% of the total mass. It was expected that energy dissipation from the sloshing fuel would cause the satellites to quickly attain a 90^0 coning angle, i.e. a flat spin about the maximum inertia axis. The satellites are essentially axisymmetric with the minimum inertia axis being the axis of symmetry (see Fig. 1). The maximum inertia axis should be located very close to the $\vec{Y}_G - \vec{Z}_G$ plane.

PROBLEM STATEMENT

The problem is to derive each satellite's motion characteristics which are needed to validate and interpret satellite system and mission performance.

ATTITUDE RELATED DATA

Three-axis magnetometer data are telemetered real time, during contacts, at the rate of 8 samples/second. Fig. 2 illustrates the magnetometer data histories (MAGX, MAGY and MAGZ along the X, Y and Z axes) for a 7 minute contact with vehicle 2 on revolution (Rev) 20.4, approximately 1.3 days after launch. The dropouts and wild points have not been removed from the illustrated data. The equal periodicity on each axis, and the small amplitude in the MAGZ data, indicate that the satellite is indeed in a flat spin about an axis very near the Z-axis of the satellite. Both vehicles achieved a flat spin prior to the first telemetry contact which occurred approximately one hour after launch.

The telemetry data is a) processed real time for CRT display and associated hardcopy output, and b) stored on an analog tape for optional post-pass processing. Both processing methods convert the raw magnetometer data to engineering units using calibration curves derived on the ground prior to launch. The quantization interval, in engineering units, is $0.472\,\mu$T. Real-time hardcopy output of the magnetometer data at a rate of 1 sample/second is routinely available. Since post-pass analog tape processing is expensive, a ground-rule was established that the analysis process be compatible with use of the real-time hardcopy output.

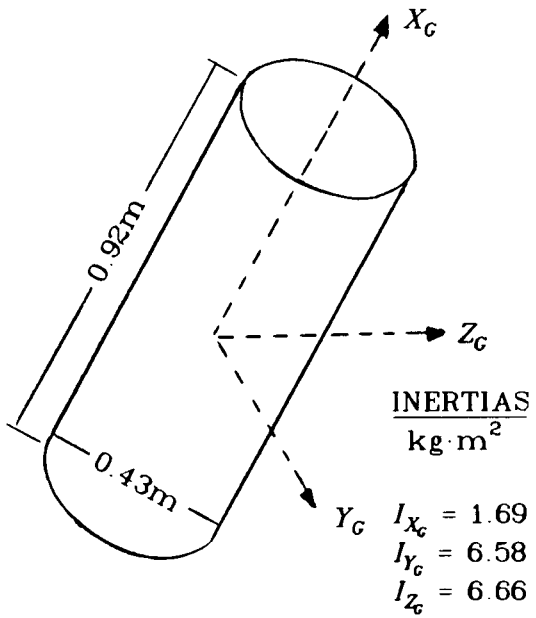

Fig. 1 Satellite Configuration

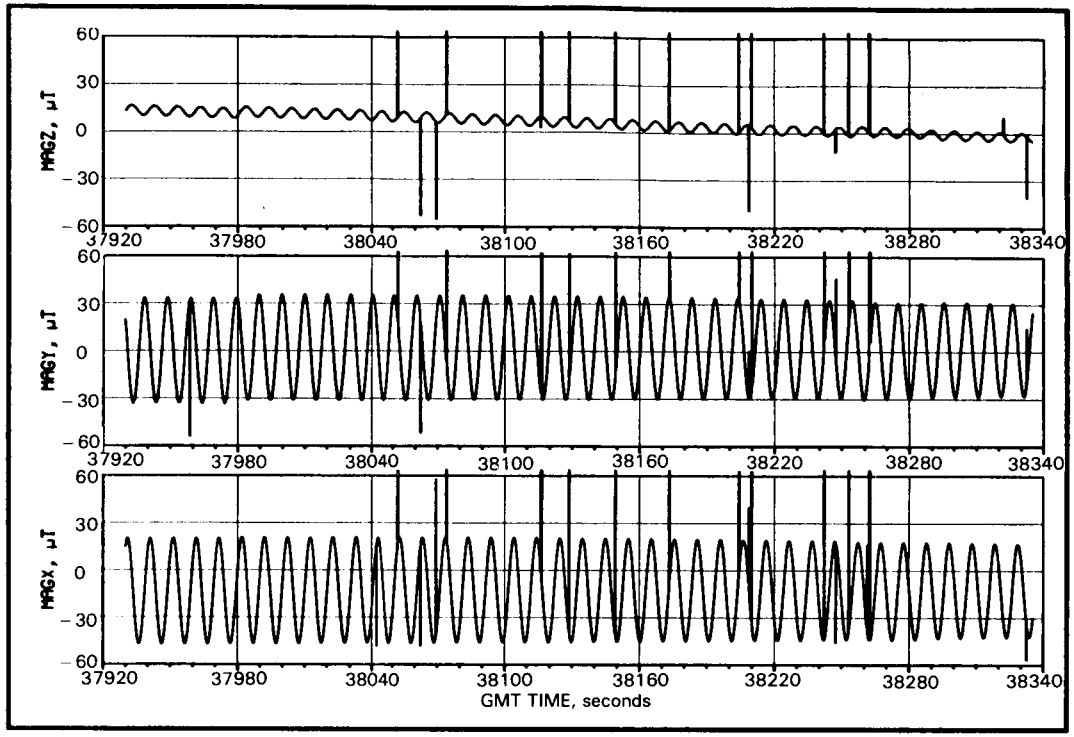

Fig. 2 Magnetometer Histories for Rev 20.4, Vehicle 2

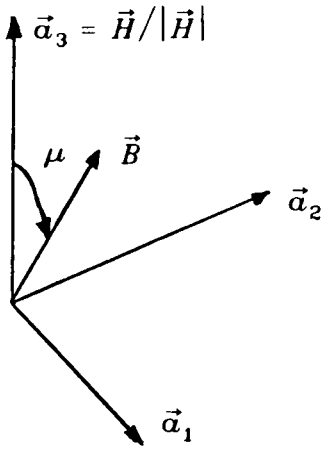

Fig. 3 Instantaneous Coordinate System

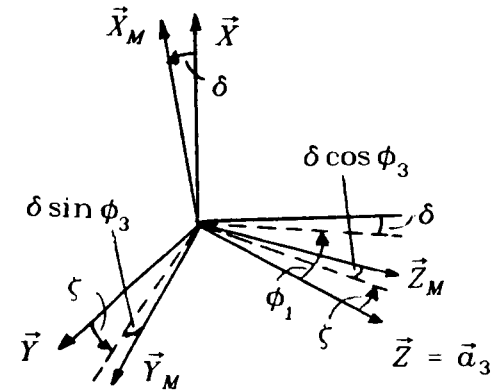

Fig. 4 Relationship Between Principal and Magnetometer Coordinates

ANGULAR MOMENTUM, SINGLE CONTACT

External torques acting on the orbiting satellites are small. Thus, during a short contact, the angular momentum $\vec{H}$ (referenced to an inertial Newtonian frame) may be assumed to be constant. At a given time t, let $\vec{B}(t)$ be the magnetic induction vector, and establish a coordinate system $\vec{a}_1(t), \vec{a}_2(t)$, and $\vec{a}_3$ of mutually perpendicular unit vectors satisfying:

$\vec{a}_3$ is parallel to $\vec{H}$,
$\vec{a}_2(t)$ is parallel to $\vec{a}_3 \times \vec{B}(t)$, and
$\vec{a}_1(t) = \vec{a}_2(t) \times \vec{a}_3$.

The geometry at a given instant in time is illustrated in Fig. 3. Let $\mathcal{P} = (\vec{X}\ \vec{Y}\ \vec{Z})$ be the principal axes coordinate system of the vehicle with $\vec{Z}$ the maximum inertia axis and $\vec{X}$ the minimum inertia axis. For flat spin motion, $\vec{Z}$ is parallel to $\vec{H}$, i.e. $\vec{Z} = \vec{a}_3$. The relationship between the vehicle magnetometer coordinate system $\mathcal{M} = (\vec{X}_M\ \vec{Y}_M\ \vec{Z}_M)$ and $\mathcal{P}$ is illustrated in Fig. 4. The magnetometer axes are designed to be mutually orthogonal and oriented along the vehicle geometric, $\mathcal{G}$, frame. The magnetometer data gives no information on the $\mathcal{G}$ frame. We thus work with the $\mathcal{M}$ frame and assume it is an orthogonal system.

The vehicle motion in principal axes is described by:

$$\begin{aligned} \vec{X}(t) &= \vec{a}_1(T_o)\cos(\Omega_p t + \psi_o) + \vec{a}_2(T_o)\sin(\Omega_p t + \psi_0) \\ \vec{Y}(t) &= -\vec{a}_1(T_o)\sin(\Omega_p t + \psi_0) + \vec{a}_2(T_o)\cos(\Omega_p t + \psi_0) \\ \vec{Z}(t) &= \vec{a}_3 \end{aligned} \tag{1}$$

where

Ω_p is the precession rate,
ψ_o is the initial precession angle,
T_o is the initial time,
T is the current time, and
$t = T - T_o$.

In the $\mathcal{M}$ frame, making the small angle approximation for δ and setting $\cos\delta$ to 1:

$$\begin{aligned} \vec{X}_M(t) &= \vec{X}(t) + \delta\sin\phi_1\,\vec{Y}(t) - \delta\cos\phi_1\,\vec{Z}(t) \\ \vec{Y}_M(t) &= \delta\sin\phi_3\,\vec{X}(t) + \cos\zeta\,\vec{Y}(t) + \sin\zeta\,\vec{Z}(t) \\ \vec{Z}_M(t) &= \delta\cos\phi_3\,\vec{X}(t) - \sin\zeta\,\vec{Y}(t) + \cos\zeta\,\vec{Z}(t) \end{aligned} \tag{2}$$

where

ϕ_1, δ and ϕ_3 are the Euler angle rotations about the X, Y and X axes, respectively, and
$\zeta = \phi_1 + \phi_3$. (See Fig. 4.)

The vehicle's spin period is short relative to its translational motion. Thus we assume that $\vec{B}$, and therefore $\vec{a}_1$ and $\vec{a}_2$, are constant over one spin cycle. Then the magnetometer history over one cycle satisfies:

$$\begin{aligned}
\vec{X}_M \cdot \vec{B} &= |\vec{B}| \left[-\delta \cos\mu \cos\phi_1 - \delta \sin\mu \sin\phi_1 \sin(\Omega_p t + \psi_o) + \sin\mu \cos(\Omega_p t + \psi_o) \right] \\
\vec{Y}_M \cdot \vec{B} &= |\vec{B}| \left[\cos\mu \sin\zeta - \sin\mu \cos\zeta \sin(\Omega_p t + \psi_o) + \delta \sin\mu \sin\phi_3 \cos(\Omega_p t + \psi_o) \right] \\
\vec{Z}_M \cdot \vec{B} &= |\vec{B}| \left[\cos\mu \cos\zeta + \sin\mu \sin\zeta \sin(\Omega_p t + \psi_o) + \delta \sin\mu \cos\phi_3 \cos(\Omega_p t + \psi_o) \right]
\end{aligned} \tag{3}$$

The extrema, $\vec{E}^{\pm}$, in (3) are:

$$E^{\pm}_{X_M} = |\vec{B}| \left[\pm \sin\mu - \delta \cos\mu \cos\phi_1 \right] \tag{4a}$$

$$E^{\pm}_{Y_M} = |\vec{B}| \left[\pm \sin\mu \cos\zeta + \cos\mu \sin\zeta \right] \tag{4b}$$

$$E^{\pm}_{Z_M} = |\vec{B}| \left[\pm \sin\mu \sin\zeta + \cos\mu \cos\zeta \right] \tag{4c}$$

The extrema, $\tilde{E}^{\pm}$, in the observed values, assuming no scaling errors, are:

$$\tilde{E}^{\pm} = \vec{E}^{\pm} + \vec{D} \tag{5}$$

where

$\vec{D} = \begin{pmatrix} D_{X_M} \\ D_{Y_M} \\ D_{Z_M} \end{pmatrix}$ are the biases along the magnetometer axes.

The derivatives of (3) are:

$$\begin{aligned}
\frac{d\,\vec{X}_M \cdot \vec{B}}{dt} &= -\Omega_p |\vec{B}| \sin\mu \left[\delta \sin\phi_1 \cos(\Omega_p t + \psi_o) + \sin(\Omega_p t + \psi_o) \right] \\
\frac{d\,\vec{Y}_M \cdot \vec{B}}{dt} &= -\Omega_p |\vec{B}| \sin\mu \left[\cos\zeta \cos(\Omega_p t + \psi_o) + \delta \sin\phi_3 \sin(\Omega_p t + \psi_o) \right] \\
\frac{d\,\vec{Z}_M \cdot \vec{B}}{dt} &= \Omega_p |\vec{B}| \sin\mu \left[\sin\zeta \cos(\Omega_p t + \psi_o) - \delta \cos\phi_3 \sin(\Omega_p t + \psi_o) \right]
\end{aligned} \tag{6}$$

The occurrences of the extrema are summarized below:

$$\vec{X}_M \cdot \vec{B} : \tan(\Omega_p t + \psi_o) = -\delta \sin\phi_1 \tag{7a}$$

$$\vec{Y}_M \cdot \vec{B} : \tan(\Omega_p t + \psi_o) = -\cos\zeta / \delta \sin\phi_3 \tag{7b}$$

$$\vec{Z}_M \cdot \vec{B} : \tan(\Omega_p t + \psi_o) = \sin\zeta / \delta \cos\phi_3 \tag{7c}$$

Equation 7c is particularly useful in determining δ when ζ and ϕ_3 are small. In this case $\zeta \approx \phi_1$. Note that Equation 7a is ≈ 0.

Procedure

1) Obtain μ from the amplitude in $\vec{X}_M \cdot \vec{B}$ (Equation 4a).
2) Obtain ζ from either $\vec{Y}_M \cdot \vec{B}$ or $\vec{Z}_M \cdot \vec{B}$, whichever has the smaller amplitude (Equation 4b or 4c).
3) Equations 7b and 7c yield approximations to δ and ϕ_3 from inexact values of t determined from the magnetometer data.
4) Determine $\vec{E}^{\pm}$ from Equation 4.
5) Determine $\vec{D}$ from Equation 5.

If $\sin\mu \approx 1$, then an accurate value of μ or $\vec{D}$ cannot be obtained. The best procedure here is to assume $\sin\mu = 1$, perform steps 2) and 3), and use an average value of $\vec{D}$ from other contacts to solve for $\cos\mu$ from either of Equations 4b or 4c. With the exception of this case, the magnetometer biases need not be a priori known to solve for μ and ζ.

Determination of Quadrant

The following rules resolve the quadrants of ζ and μ:

$$\begin{aligned} \operatorname{sgn}(\sin\zeta) &= \operatorname{sgn}\left(\frac{d\,\vec{X}_M \cdot \vec{B}}{dt}\right) \text{ at } t \text{ maximizing } \vec{Y}_M \cdot \vec{B}\,. \\ \operatorname{sgn}(\cos\zeta) &= \operatorname{sgn}\left(\frac{d\,\vec{X}_M \cdot \vec{B}}{dt}\right) \text{ at } t \text{ maximizing } \vec{Z}_M \cdot \vec{B}\,. \\ \operatorname{sgn}(\cos\mu) &= \operatorname{sgn}\left(\overline{\vec{Z}_M \cdot \vec{B}}\right)\operatorname{sgn}(\sin\zeta)\,. \end{aligned} \tag{8}$$

Effect of $\vec{B}$ Variation with Time

In practice, fixing $\vec{B}$ has little effect on the solutions for μ, ζ and δ. The variation in $\vec{B}(t)$ is important in the determination of Ω_p:

$$\Omega_p = \tilde{\Omega}_p + \frac{d\,\vec{\alpha}_2(t)}{dt} \tag{9}$$

Specifically, the observed precession rate, $\tilde{\Omega}_p$, can be quite different from Ω_p if $\vec{H} \cdot \vec{B}$ is small. Further, the values of $\vec{\alpha}_2(t)$ for the two solutions of $\vec{H}$ are opposite in sign.

Example 1: $\sin\mu$ is Small

Table 1 gives results for the contact on Rev 164 with vehicle 2. The telemetered magnetometer histories are illustrated in Fig. 5. The $\vec{B}$ values were obtained from an orbit simulation code using a 12 degree spherical harmonic expansion for the geomagnetic potential. The algorithms are used to compute ζ, μ, $(\vec{E}^+ + \vec{E}^-)/2$, $\vec{D}$ and δ. Independent estimates, $\hat{D}$, for the biases, for comparison purposes, were obtained by an estimation scheme which minimizes, in a least squares sense, the difference between the magnitudes of the bias-adjusted measured vector and the modelled magnetic induction vector. The value of the biases vary with the operating configuration of the satellite which is slightly different for each of the three times. The accuracy in δ is poor because of the small variation in $\vec{Z}_M \cdot \vec{B}$ and the large quantization interval. The offset in the extrema of $\vec{Z}_M \cdot \vec{B}$ from $\vec{X}_M \cdot \vec{B}$ and $\vec{Y}_M \cdot \vec{B}$ is illustrated in Fig. 6 for Rev 20.4 which gives a larger variation in $\vec{Z}_M \cdot \vec{B}$. The satellite rotates about 64° between the occurrences of the $\vec{X}_M \cdot \vec{B}$ and $\vec{Z}_M \cdot \vec{B}$ maxima. This angle was used in Equation 7c to solve for δ assuming ϕ_3 is 0. Analysis of several contacts indicated that the values for ζ and δ were close to 5° and 2°, respectively. When used in Equations 4 and 5, these yield a value of $\vec{D}$ which agrees very closely with $\hat{D}$.

Example 2: $\sin\mu \approx 1$

It is difficult to determine μ accurately when $\sin\mu \approx 1$. Table 2, pertaining to the contact on Rev 20.4 of vehicle 2, illustrates the procedure described above. (Refer to Fig. 2 for the magnetometer histories.) First obtain estimates, $\hat{\mu}$ and $\hat{D}$, of μ and D. Equation 4a is used to determine $\hat{\mu}$. In general, $\hat{D}$ is an average over several selected contacts. (The value of $\hat{D}$ used in Table 2 was obtained using the aforementioned bias estimation code since the analog tape for that contact was processed post-pass.) Then $\vec{E}^{\pm}$ is determined from Equation 5 and μ is computed more accurately from (4c) in the form:

$$\cos\mu = \frac{\vec{E}^+ + \vec{E}^-}{2\,|\vec{B}|\cos\zeta}$$

where ζ is obtained by the usual procedure, but using $\hat{\mu}$. The other components of $\vec{D}$ now agree fairly well with those of $\hat{D}$.

TABLE 1 COMPUTATIONS FOR REV 164.2, VEHICLE 2

	T = 82849s, GMT			T = 83029s, GMT			T = 83179s, GMT		
	X	Y	Z	X	Y	Z	X	Y	Z
$\tilde{E}^+$	-5.2	10.6	38.2	-10.3	7.4	43.0	-6.6	11.3	45.3
$\tilde{E}^-$	-22.8	-7.0	36.3	-17.0	0.7	42.3	-20.6	-2.6	44.0
$\lvert\vec{B}\rvert$		27.62			30.39			32.92	
ζ		6.2			6.0			5.3	
δ		3.0			2.9			2.6	
μ		18.6			6.3			12.3	
$\overline{\vec{E}^{\pm}}$	-1.36	2.82	26.02	-1.52	3.16	30.04	-1.46	2.97	32.03
$\vec{D}$	-12.64	-1.02	11.23	-12.13	0.89	12.61	-12.15	1.38	12.62
$\hat{D}$	-13.17	0.15	11.30	-12.62	1.61	12.55	-12.62	1.61	12.55

TABLE 2 COMPUTATIONS FOR REV 20.4, VEHICLE 2

	T = 37941s, GMT			T = 38147s, GMT			T = 38327s, GMT		
	X	Y	Z	X	Y	Z	X	Y	Z
$\tilde{E}^+$	20.4	33.7	16.1	20.3	34.6	8.5	17.0	30.7	0.8
$\tilde{E}^-$	-47.4	-33.3	9.8	-45.7	-30.8	2.3	-42.7	-28.4	-4.8
$\lvert\vec{B}\rvert$		34.09			33.92			33.32	
$\hat{D}$	-13.53	0.17	12.48	-13.08	2.64	13.47	-13.20	2.32	13.05
$\hat{\mu}$		90.			103.4			116.4	
$\overline{\vec{E}^{\pm}}$	0.03	0.03	0.47	0.38	-0.74	-8.07	0.45	-1.17	-15.05
ζ		5.3			5.4			5.3	
δ		2.6			2.6			2.6	
μ		89.2			103.8			117.0	
$\vec{D}$	-13.47	0.15	12.48	-13.09	2.66	13.47	-13.43	2.55	-15.05

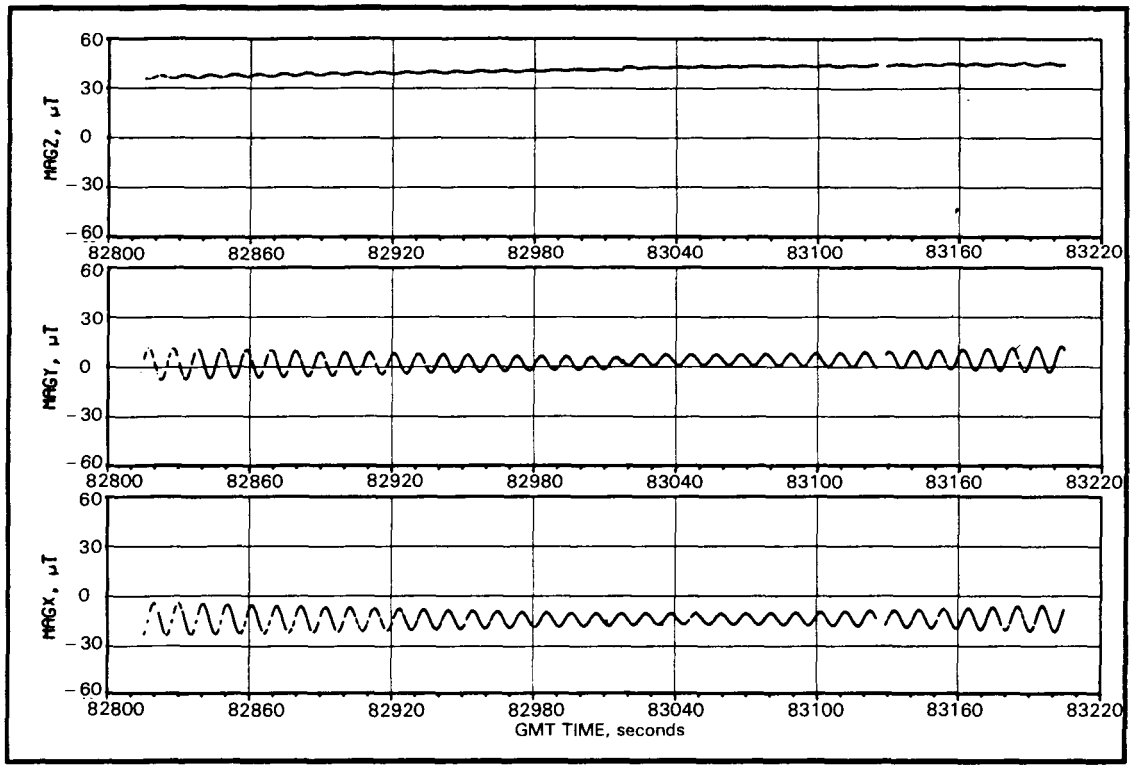

Fig. 5 Magnetometer Histories for Rev 164.2, Vehicle 2

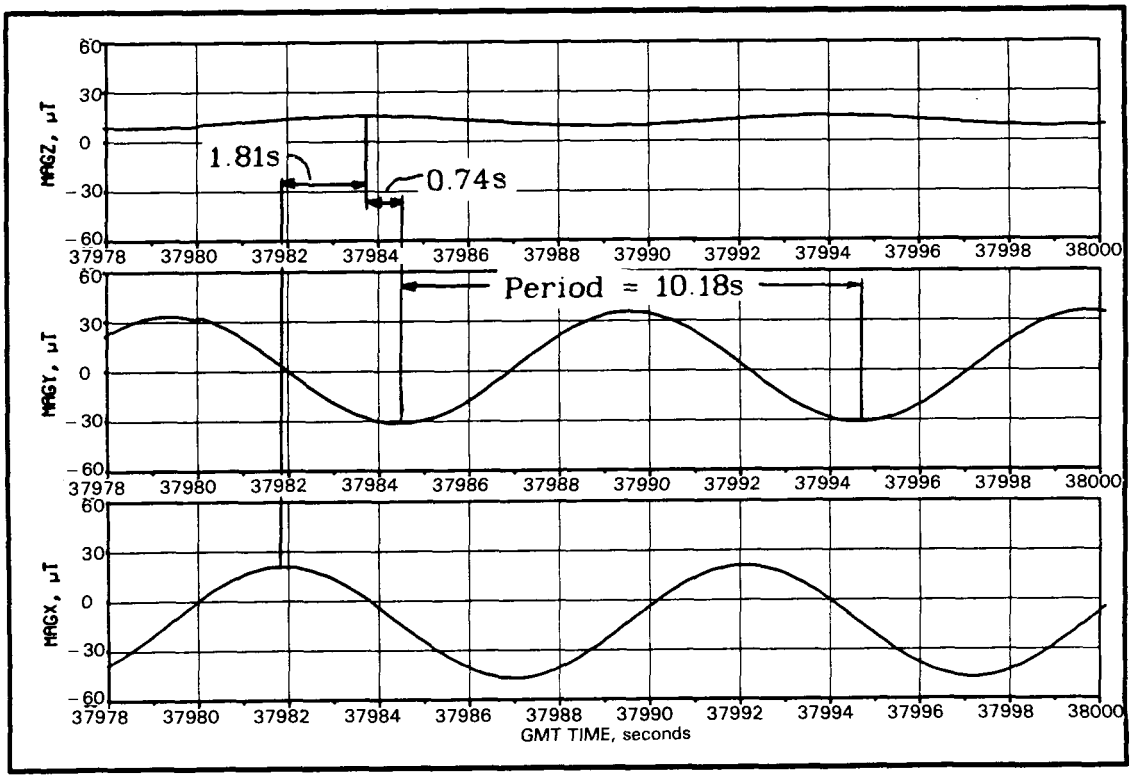

Fig. 6 Magnetometer Cycle Offset for Rev 20.4, Vehicle 2

Ambiguity in $\vec{H}$

The procedure described above resolves $\vec{H}$ to lie on a cone of angle μ about $\vec{B}$. As the geometry, specifically $\vec{B}$, varies with time due to satellite orbital motion, $\vec{H}$ can be resolved to two points: the intersection of two cones. Over a short contact, the magnetic induction vectors are essentially co-planar. The two possible $\vec{H}$ vectors are the true $\vec{H}$ and its mirror image relative to the '$\vec{B}(t)$ plane'.The key point is that $\vec{H}$ cannot be uniquely determined over a short contact. This can be observed very readily in Fig. 7 which illustrates the loci of possible $\vec{H}$ (minor circles of radius μ_i about point Bi which is the intersection of $\vec{B}_i$ with the unit sphere) in right ascension and declination at the three times in Table 1. (A Kalman filter estimation technique designed specifically for this problem could not, in general, decide which of the two possibilities was the correct $\vec{H}$ orientation.)

The geometry of the two possible $\vec{H}$ solutions will vary with the orientation of the actual $\vec{H}$ with respect to the $\vec{B}$ vectors during the contact. For Rev 21.4, vehicle 1 (Fig. 8), $\vec{H}$ is quite far from the 'plane' of the $\vec{B}(t)$ vectors so that the two $\vec{H}$ possibilities are widely separated. This contact is sufficiently long - 7 minutes - for $\vec{B}(t)$ to be non-planar which allows the correct $\vec{H}$ to be resolved. On Rev 20.1, vehicle 2 (Fig. 9), $\vec{H}$ is many degrees from $\vec{B}$ but is close to the $\vec{B}(t)$ plane so that, with the uncertainties associated with μ, the possible $\vec{H}$ values lie along an arc of $\approx 30^\circ$ encompassing declinations from -20° to -45^0. Rev 1.1 for vehicle 1 (see Fig. 10) has similar geometry.

Since the satellite contacts are short, on the order of 3 to 5 minutes, and may be separated by about 30 days, other methods must be employed to resolve the ambiguity in the angular momentum orientation. The next section discusses how this issue is resolved.

ANGULAR MOMENTUM RESOLUTION

Resolution of the correct angular momentum orientation between the two possibilities requires a) an initial orientation for $\vec{H}$, and b) a torque model from which a long-term history of $\vec{H}$ can be derived.

Initial Orientation of $\vec{H}$

There were frequent contacts with the satellites during the first few days in orbit. Fig. 10 illustrates a resolved orientation for the $\vec{H}$ of vehicle 1 at the intersection of the loci for contacts on Revs 1 and 2. This solution is essentially

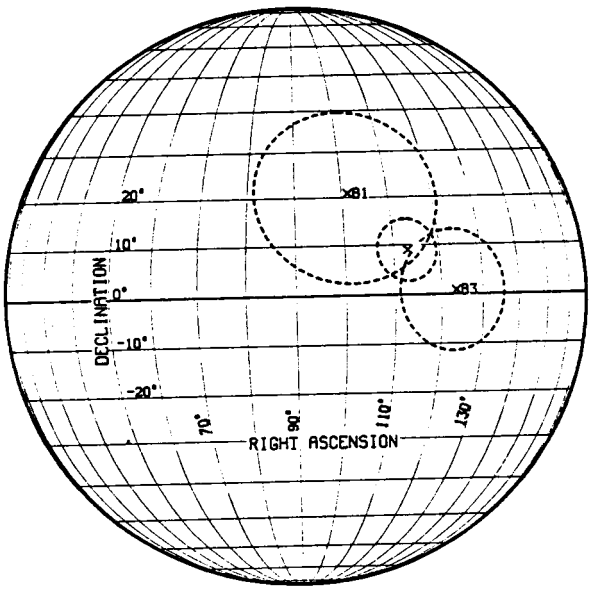

Fig. 7 Potential $\vec{H}$ Orientations:
Rev 164.2, Vehicle 2

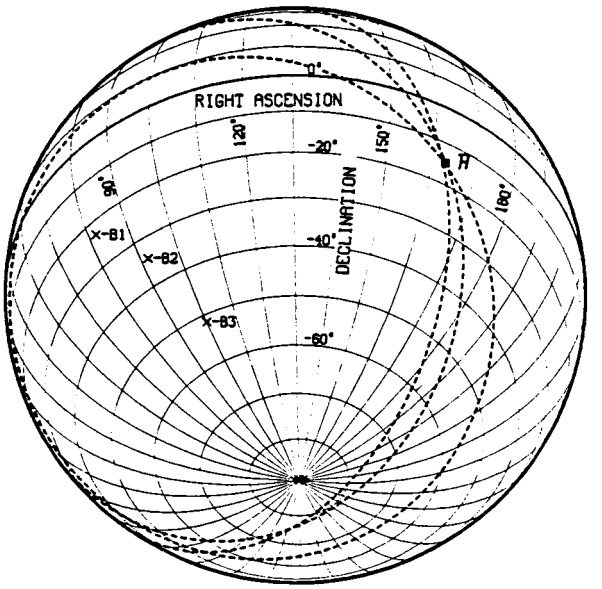

Fig. 8 Resolved $\vec{H}$ Orientation:
Rev 21.4, Vehicle 1

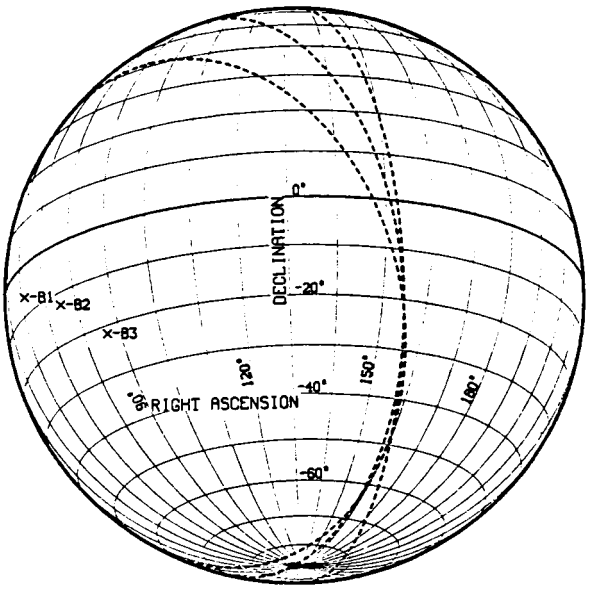

Fig. 9 Potential $\vec{H}$ Orientations:
Rev 20.4, Vehicle 2

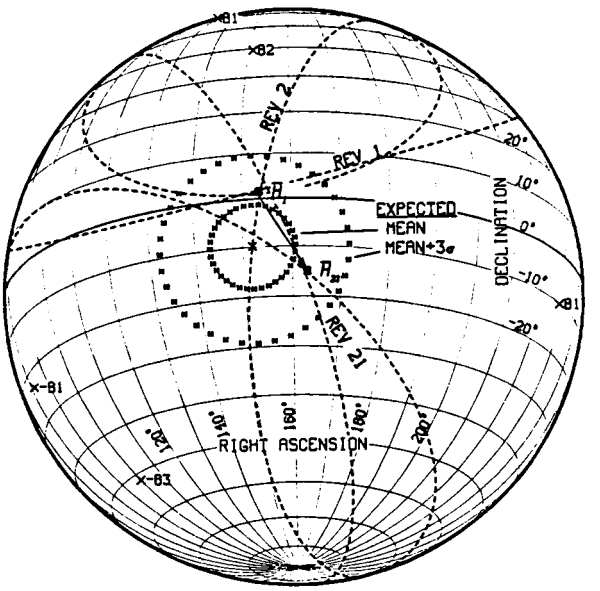

Fig. 10 Resolved $\vec{H}$ Orientations:
Days 1-2, Vehicle 1

on the mean of the expected loci determined by a statistical analysis, conducted pre-launch, of the separation of the satellites from the 4th Stage of the launch vehicle. Fig. 10 illustrates a likely $\vec{H}$ path from this solution to the $\vec{H}$ solution on Rev 21. This corresponds to a precession in $\vec{H}$ of $\approx 15^{\circ}/\text{day}$.

The initial orientation of $\vec{H}$ for vehicle 2 was established at a right ascension of 162° and a declination of -30°

Torque Model

Torques acting on the orbiting satellites originate from magnetic, gravity gradient, aerodynamic, and solar radiation pressure effects. The approach taken was to obtain expressions, available in the published literature, for the effect, on $\vec{H}$, of each significant torque over one satellite revolution. These expressions, along with a dipole model of the earth's magnetic field[5] were incorporated into a semi-anlytic orbit generation code using a 1-rev step-size. The torque expressions are described briefly below. Because of the small size of the satellites, solar radiation pressure was judged to be a relatively insignificant contributor and was not included in the model.

Magnetic Torques: - Magnetic torques result from the interaction between the magnetic properties of a spacecraft and the ambient magnetic field of the earth. The primary magnetic disturbance torques are:

1. Dipole moment from the permanent magnetism in the spacecraft;
2. Eddy currents induced when a conducting body moves in a magnetic field;
3. Spacecraft generated current loops; and
4. Hysteresis damping.

Because of the limited amount of spacecraft operating time and the specific amount and properties of permeable material present on the spacecraft, items 3. and 4. were judged to have small contributions to total vehicle torque and were not included in the model.

The torque, $\vec{T}_D$, due to the dipole moment is normal to $\vec{a}_3 = \vec{H}/|\vec{H}|$, and hence has only a precession component. It satisfies[2,3,5]:

$$\vec{T}_D = m_d \vec{a}_3 \times \vec{B} \tag{10}$$

where

m_d is the satellite's dipole moment along its Z-axis.

Making the assumption that the satellite Z-axis is inertially fixed for an orbital period, the average torque over one orbit rev satisfies:

$$\left(\vec{T}_D\right)_{av} = m_d \vec{a}_3 \times (\vec{B})_{av} \tag{11}$$

$(\vec{B})_{av}$ can be integrated with respect to time over an orbital period[2] to give an average induction vector.

The total torque due to eddy current effects satisfies[5]:

$$\vec{T}_E = k_e\left(\vec{\omega}_Z \times \vec{B}\right) \times \vec{B} \tag{12}$$

where

k_e is a constant which depends on the geometry and conductivity of the rotating object, and

$\vec{\omega}_Z$ is the angular velocity vector of the satellite.

Equation (12) can be separated into despin, T_{EZ}, and precession, $T_{E\perp}$, components of torque:

$$T_{EZ} = -k_e(B_\perp)^2\omega_Z \tag{13}$$

$$T_{E\perp} = k_e B_Z B_\perp \omega_Z \tag{14}$$

where

$B_\perp$ is the component of $\vec{B}$ orthogonal to $\vec{Z}$,

B_Z is the component of $\vec{B}$ parallel to $\vec{Z}$, and

ω_Z is the angular velocity.

These equations are conceptually simple. The complication arises in finding the average values for $(B_\perp)^2$ and $B_Z B_\perp$ over one revolution of the satellite. Reference 3 derived equations for $B_\perp$ and B_Z and then integrated the resulting products. It is easier to a) resolve $\left(\vec{\omega}_Z \times \vec{B}\right) \times \vec{B}$ into its three components, b) integrate, and then c) compute the despin and orthogonal components, $(T_{EZ})_{av}$ and $(T_{E\perp})_{av}$, of torque. Since the orbit eccentricity is small, terms of $o(e^3)$ and $o(e^4)$ can be deleted.

Gravity Gradient Torque: - The average torque over one orbit due to the effect of the earth's gravitation on the satellite is[1,2,3,4]:

$$\left(\vec{T}_G\right)_{av} = 1.5\frac{\mu_E}{a^3(1-e^2)^{1.5}}\left(I_Z - \frac{I_X + I_Y}{2}\right)\left(\vec{a}_3 \cdot \vec{N}\right)\left(\vec{a}_3 \times \vec{N}\right) \tag{15}$$

where

μ_E is the earth's gravitational constant,

a is the semi-major axis of the orbit,

e is the eccentricity of the orbit, and

$\vec{N}$ is the unit normal to the orbit plane.

Aerodynamic Torque: - The average aerodynamic torque over one satellite spin cycle satisfies:

$$\vec{T}_A = \frac{1}{2}\rho v^2 S C_D d\left(\vec{I}_v \times \vec{a}_3\right) \tag{16}$$

where

ρ is the density of the atmosphere,
v is the velocity of the satellite,
S is the projected area in the direction of motion averaged over one satellite rotation,
C_D is the drag coefficient,
d is the distance from the center of mass of the satellite to its aerodynamic center of pressure along $\vec{Z}$ averaged over one satellite rotation, and
$\vec{I}_v$ is the unit velocity vector of the satellite.

The average torque over one orbit was determined using a relatively common procedure[3] for somewhat elliptical orbits.

Spin-axis Rate Change in One Orbit Revolution: - Assuming that the vehicle is in a pure spin motion about the body Z-axis, i.e. the principal inertia axis, the change in the spin rate in one orbit revolution caused by the eddy current torque is:

$$\Delta\omega_Z = -\left|\left(T_{EZ}\right)_{av}\right| \omega_Z P / I_Z \tag{17}$$

where

I_Z is the moment of inertia about the body Z-axis, and
P is the satellite orbital period.

Spin-axis Precession in One Orbit Revolution: - Over one orbit rev, the angular momentum vector, $\vec{H}$, precesses by the angle $\left|\vec{T}_{av}\right|/\omega_Z I_Z$ from $\vec{H}$ towards $\vec{T}_{av}$ where $\vec{T}_{av}$ is the sum of the individual torque contributors normal to $\vec{H}$.

RESULTS

With the incorporation of the torque model into the orbit generation code, the determination of approximate values for the key torque-related vehicle-unique properties proceeded rapidly using an iterative simulation process. The inertia properties given in Fig. 1 and an aerodynamic lever arm, d, of 0.75 cm, equal to the pre-flight measured c.g.-offset along the Z_G-axis, were used initially for both vehicles. Though they were varied to determine sensitivities, these values were used in the final simulation. The derived magnetic properties are summarized in Table 3.

TABLE 3 DERIVED MAGNETIC PROPERTIES

VEHICLE	DIPOLE MOMENT, m_d $A-m^2$	k_e m^4/ohm
1	+0.543	465
2	-0.230	465

The dipole moment values are within expectations since satellite magnetic properties were minimally controlled during the design process. The k_e constant should be the same for both vehicles. The derived value is reasonably close to the 600 m^4/ohm value computed pre-flight. The histories of the orientation of $\vec{H}$ over the first six months in orbit are illustrated in Figures 11 and 12 for vehicles 1 and 2 respectively. Over this period, the maximum differences between the simulated and calculated $\vec{H}$ orientations were one day ($\approx$15 revs) in-track (parallel to the trace of $\vec{H}$), and $\approx 10^\circ$ cross-track (normal to the trace of $\vec{H}$). Generally the agreement was much better. Fig. 13 illustrates, for Rev 3056 of vehicle 2, typical agreement between the simulation and computations for the orientation of $\vec{H}$.

The simulated spin rate histories are summarized in Figures 14 and 15. They match the 'observed' data very well except for the first few days where the differences are attributed to residual angular momentum in the hydrazine fuel. There appears to be no significant hysteresis in the material magnetization cycle. This would be manifested as a constant component to the primarily exponential spin decay rate.

Figures 16 and 17 illustrate the histories of the angles between $\vec{H}$ and $\vec{N}$. For vehicle 1, $\vec{H}$ is never more than 20° out of the orbit plane. Its projected area along the flight path, averaged over a spin cycle, is essentially constant. For contrast, the $\vec{H}$ for vehicle 2 is at times nearly normal to the orbit plane. Thus, its average projected area along the flight path is smaller than that for vehicle 1. This correlates with observed periods of $\approx$ 5% smaller effects of drag on vehicle 2.

Finally, Figures 18 and 19 illustrate the dynamic history of the sun aspect angle. This, along with the eclipse history, are necessary inputs to an assessment of the thermal performance of the vehicles. The long thermal time constant ($\approx$9 days) of the well insulated vehicles, combined with the rapid fluctuation in the sun aspect angle, led to a very uniform internal temperature history.

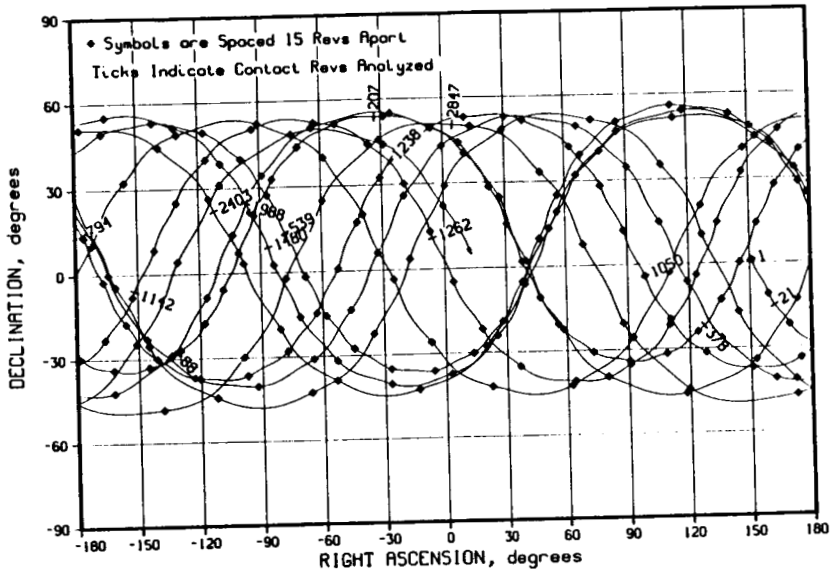

Fig. 11 Evolution of the Orientation of $\vec{H}$ for Vehicle 1

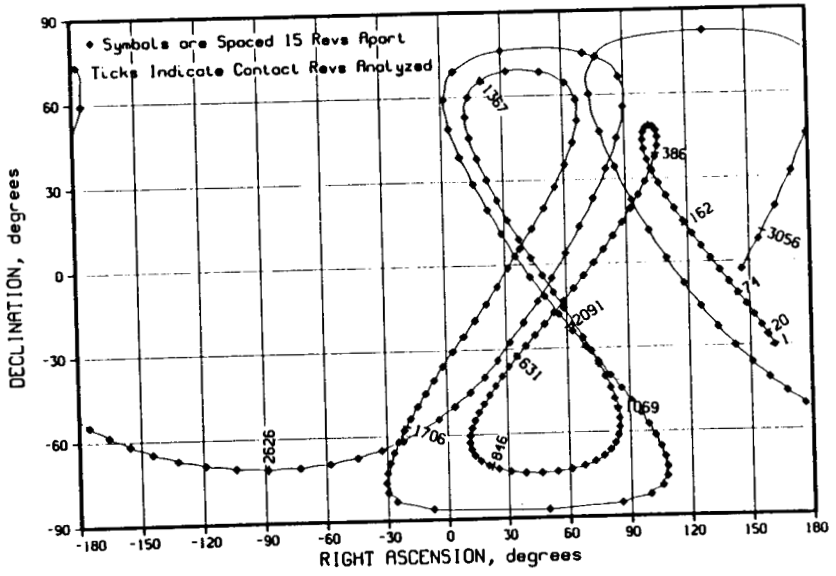

Fig. 12 Evolution of the Orientation of $\vec{H}$ for Vehicle 2

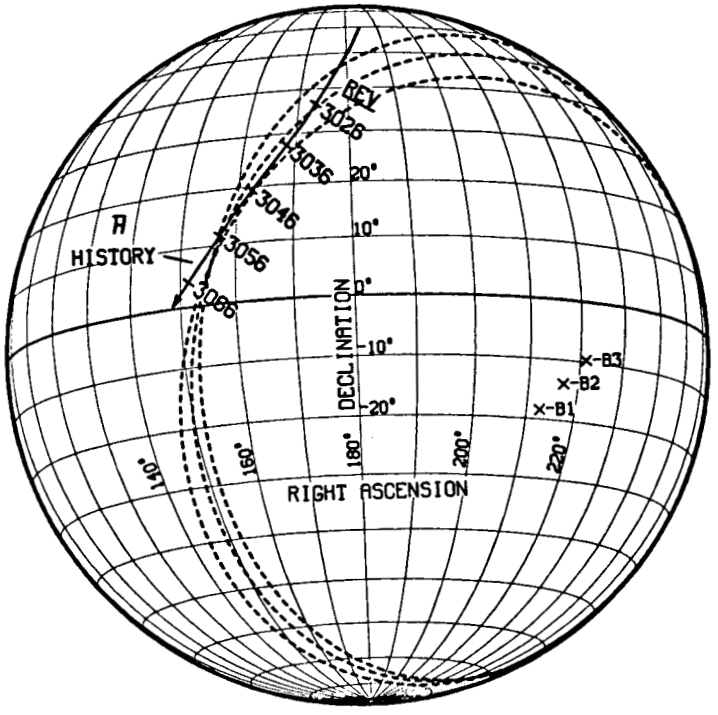

Fig. 13 Simulated vs. Resolved $\vec{H}$:
Rev 3056.2, Vehicle 2

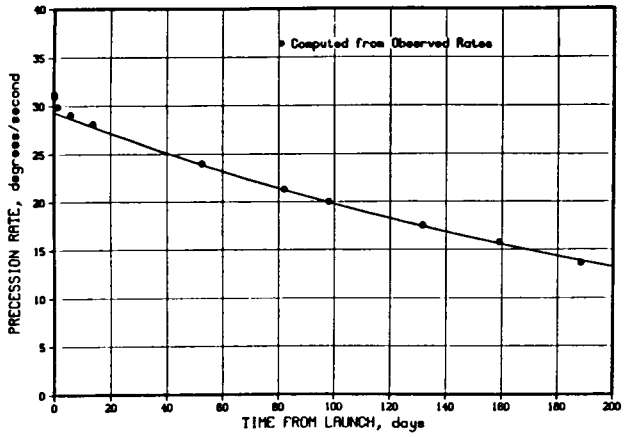

Fig. 14 Precession Rate History for Vehicle 1

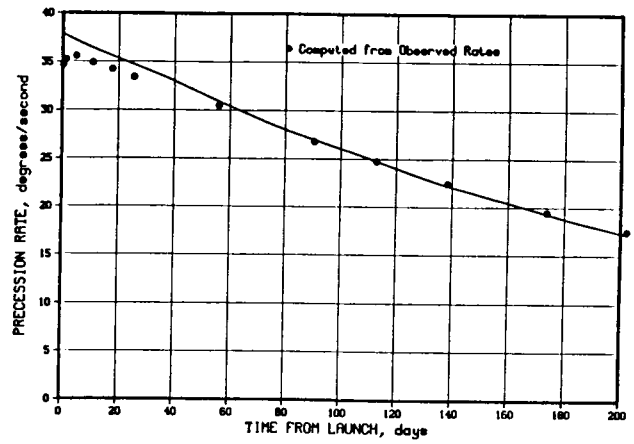

Fig. 15 Precession Rate History for Vehicle 2

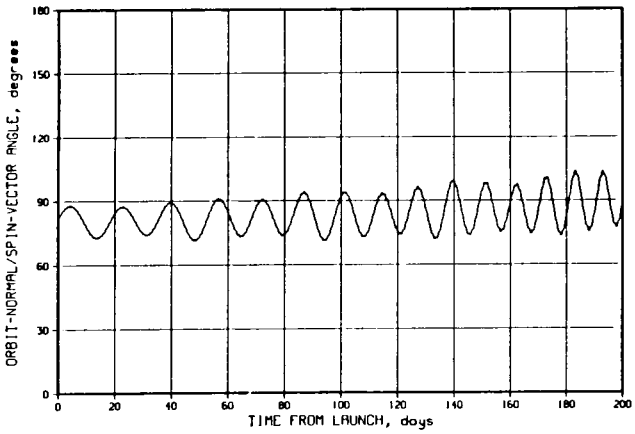

Fig. 16 Angle from $\vec{H}$ to Orbit Normal, Vehicle 1

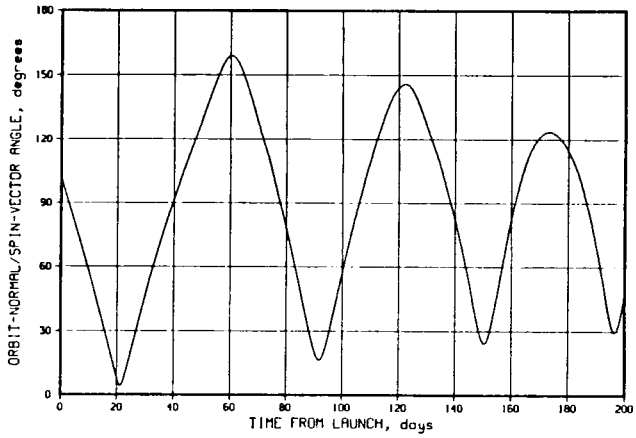

Fig. 17 Angle from $\vec{H}$ to Orbit Normal, Vehicle 2

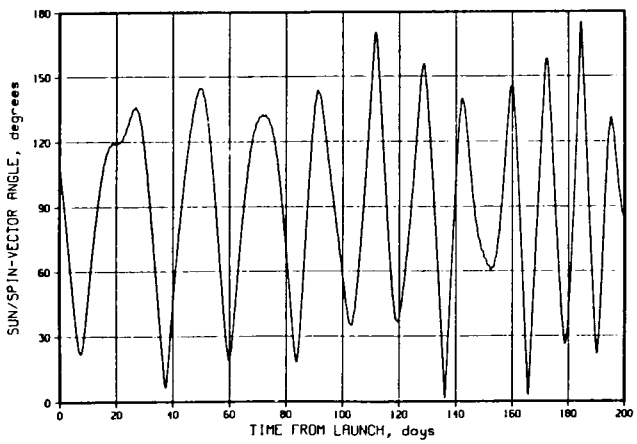

Fig. 18 Solar Aspect Angle to $\vec{H}$ for Vehicle 1

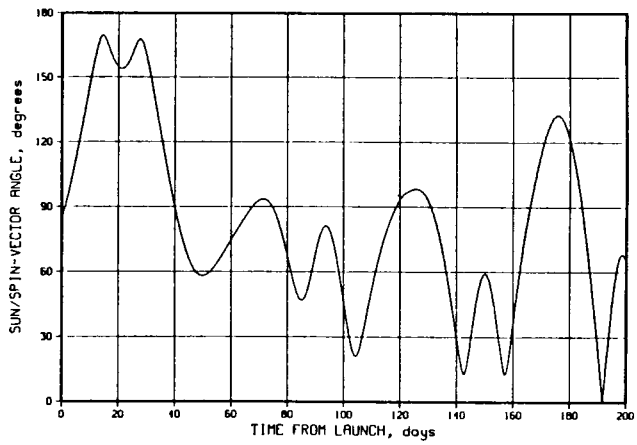

Fig. 19 Solar Aspect Angle to $\vec{H}$ for Vehicle 2

ACKNOWLEDGEMENT

The author is indebted to Mr. Richard Heldt of Synetics Corp. (formerly of Textron Defense Systems) for generating, coding, and exercising the bias estimation and Kalman filter codes.

REFERENCES

1. Hughes; Peter C. *Spacecraft Attitude Dynamics*, John Wiley & Sons, New York, 1986

2. Patapoff, H. "Attitude Drift of a Spin-Stabilized Satellite due to the Earth's Magnetic and Gravitational Fields", *Proceedings, XIVth International Astronautical Congress*, Paris, 1963

3. Renard, Marc L. "Attitude Perturbations and Magnetic Control of a Spin-Stabilized Satellite", ESRO TR-1 (ESTEC), January,1966

4. Sample, E. C. "A Study of the Spin-Axis Precession Characteristics to be Expected of the S53/UK3 Satellite", RAE Technical Note No. Space 62, April, 1964

5. "Spacecraft Magnetic Torques", NASA SP-8018, March, 1969